Histol Histopathol (2025) 40: 381-388

Histology and Histopathology
From Cell Biology to Tissue Engineering

ORIGINAL ARTICLE Open Access

Clinicopathological and molecular features of genome-stable colorectal cancers

Lingyan Jin[1,2*], Hye-Yeong Jin[1,2*], Younghoon Kim[2,3], Nam-Yun Cho[2], Jeong Mo Bae[1,2], Jung Ho Kim[1], Sae-Won Han[4], Tae-You Kim[4] and Gyeong Hoon Kang[1,2*]

[1]Department of Pathology, [2]Laboratory of Epigenetics, Cancer Research Institute, Seoul National University College of Medicine, [3]Department of Hospital Pathology, Seoul St. Mary's Hospital, College of Medicine, The Catholic University of Korea and [4]Department of Internal Medicine, Seoul National University College of Medicine, Seoul, Korea

*These authors contributed equally to this work

Summary. Colorectal cancers (CRCs) are traditionally divided into those with either chromosomal instability (CIN) or microsatellite instability (MSI). By utilizing TCGA data, the Laird team found a subset of CRCs, namely, genome-stable CRCs (GS CRCs), which lack both CIN and MSI. Although the molecular features of GS CRCs have been described in detail, the clinicopathological features are not well defined.

A total of 437 CRCs were analyzed for copy number variation (CNV) statuses in eight genes (*ARID1A*, *EGFR*, *FGFR1*, *KDM5B*, *MYBL2*, *MYC*, *SALL4*, and *SETDB1*) using droplet-digital PCR. CRCs that showed CNV in ≤ one gene and no MSI were defined as GS-like CRCs. Clinicopathological and molecular features of GS-like CRCs were compared with those of CIN-like CRCs. GS-like CRCs comprised 4.6% of CRCs and showed a predilection toward the proximal colon, lower nuclear optical density, *KRAS* mutation, *PIK3CA* mutation, and aberrant expression of KRT7. Survival analysis showed no significant difference between the three subgroups. Through our study, the GS-like subtype was found to comprise a minor proportion of CRCs and have proclivity toward a proximal bowel location, hypochromatic tumor nuclei, aberrant KRT7 expression, and a high frequency of *KRAS* and *PIK3CA* mutations.

Key words: Colorectal cancer, Molecular subtype, Chromosomal instability, Microsatellite instability, Genome stability, PIK3CA

Corresponding Author: Gyeong Hoon Kang, M.D. & Ph.D., Department of Pathology, Seoul National University College of Medicine, 103, Daehak-ro, Chongno-gu, Seoul, 03080, Korea. e-mail: ghkang@snu.ac.kr

www.hh.um.es. DOI: 10.14670/HH-18-785

Introduction

Colorectal cancer (CRC) is one of the most common malignancies in the world (Sung et al., 2021), being the third most common malignancy and the third leading cause of cancer death in Korea (http://kostat.go.kr) (Jung et al., 2022). CRC is a heterogeneous disease entity in terms of molecular carcinogenesis pathways, which include chromosomal instability (CIN), microsatellite instability (MSI), and CpG island methylator phenotype (CIMP) pathways (Pino and Chung, 2010; Al-Sohaily et al., 2012; Colussi et al., 2013; Nguyen et al., 2020). CRCs with CIN are characterized by alterations in the number and structure of chromosomes, whereas MSI-high CRCs are characterized by genome-wide alterations in repeat lengths of microsatellites and an increased rate of single nucleotide variations. MSI-high CRCs exhibit high tumor mutation burden but few gains or losses of chromosomal regions and thus could be classified as chromosome-stable CRCs, whereas CRCs with CIN are microsatellite-stable (Trautmann et al., 2006). Tumors can be broadly classified into CIN, MSI-high, or CIMP-high tumors. Recently, by utilizing The Cancer Genome Atlas (TCGA) data, the Laird team identified a subset of CRCs, genome-stable (GS) CRCs, which lack aneuploidy and MSI (Liu et al., 2018).

Morphological correlates have been demonstrated for CRCs with CIN, MSI, or CIMP (Jass, 2007; Bae et al., 2016; Shia et al., 2017). The classic adenoma-carcinoma sequence is the morphological pathway for CRCs with CIN or hereditary MSI-high CRCs, whose premalignant lesions are conventional adenomas (Jass et al., 2002). The serrated neoplasia pathway is the morphological route for sporadic MSI-high and CIMP-high CRCs, which develop through sessile or traditional serrated adenomas (Leggett and Whitehall, 2010; Satorres et al., 2021). Based on the finding of a high frequency of *APC* mutations in GS CRCs, the Laird

team suggested that GS CRCs might develop along the classic adenoma-carcinoma sequence (Liu et al., 2018). Nevertheless, no further study has elucidated the molecular or clinicopathological features of GS CRCs.

CIN and MSI statuses are easily determined based on whole-genome or whole-exome next-generation sequencing (NGS); thus, GS CRCs are not difficult to diagnose. Without NGS, however, it is difficult to diagnose (McGranahan et al., 2012; Lepage et al., 2019), contrasting with the situation for MSI or CIMP. In the present study, microsatellite-stable (MSS) tumors that showed little alteration in copy number (CN) of selected proto-oncogenes or tumor-related genes analyzed by droplet-digital PCR (ddPCR) were diagnosed as GS-like CRCs. A total of 437 CRC specimens were analyzed for their CN status in eight selected genes using ddPCR, and GS-like CRCs were correlated with clinicopathological and molecular features.

Materials and methods

Samples

A total of 437 formalin-fixed, paraffin-embedded (FFPE) CRC tissues were retrieved from the surgical files of the Department of Pathology, Seoul National University Hospital, Seoul, Korea. The patients underwent curative surgery (R0) and received oxaliplatin-based adjuvant chemotherapy for stage II or stage III CRC from 2005 to 2012. The inclusion and exclusion criteria for these patients were described in detail previously (Jin et al., 2022). Clinical and histological information was collected from electronic medical records, including tumor subsite within the large bowel, tumor grading, lymphatic embolus, perineural invasion, and tumor-node-metastasis (TNM) stage (American Joint Committee on Cancer, 7th edition). This study was approved by the Institutional Review Board of Seoul National University Hospital (H-2310-026-1474), and the requirement to obtain informed consent was waived by the Institutional Review Board of Seoul National University Hospital because this study was retrospective with minimal risks to the subject. This study was performed in accordance with the Declaration of Helsinki guidelines.

DNA isolation and quantification

The tumor areas with the highest tumor purity and most representative histology of the case were marked on the tissue slides under the microscope, and the corresponding areas were manually dissected from three to five unstained serial sections (10 μm thick). The dissected tissues were collected and subjected to a DNA extraction process using the QIAamp DNA FFPE Tissue kit (Qiagen, Carlsbad, CA). Purified genomic DNA was quantified with a Qubit 2.0 fluorometer (Thermo Scientific, Wilmington, DE, USA).

Analysis of BRAF, KRAS, TP53, and PIK3CA mutations

BRAF mutations at codon 600 (V600E) were analyzed with pyrosequencing (n=432), as previously described (Spittle et al., 2007). The PCR and sequencing primer sequences were as follows: forward, 5′-TTCATGAAGACCTCACAGTAAAAAT-3′; reverse, 5′-biotin- GCATCTCAGGGCCAAA-3′; sequencing forward, 5′- GGTGATTTTGGTCTAGCTAC-3′. The amplicons were sequenced using PyroMark Gold reagents (Qiagen) on a PyroMark Q24 (Qiagen). Sanger sequencing of *KRAS* exon 2 was performed to identify the mutation status of codons 12 and 13 (n=435). The PCR primer sequences for *KRAS* exon 2 were as follows: forward, 5'-ACTGAATATAAACTTGTGGT AGTTGGCCCT-3'; reverse, 5'-AACAAGATTTACCT CTATTGTTGGATCA-3'. The tumors (n=348) were previously analyzed for their mutation status in 40 genes, including *PIK3CA* and *TP53*, and *KRAS* exons 3 and 4 using NGS (Lee et al., 2017).

MSI analysis

MSI status was determined in each tumor using PCR amplification with fluorescently labeled primers (BAT25, BAT26, D2S123, D5S346, and D17S250). Each tumor was classified as MSI-high (≥2 unstable markers), MSI-low (one unstable marker), or MSS (no unstable marker).

CIMP analysis

The genomic DNA samples were bisulfite-modified using an EZ DNA methylation kit (Zymo Research, Irvine, CA, USA). Bisulfite-modified DNA was subjected to MethyLight analysis, which assessed the methylation status of eight CIMP markers (*CACNA1G*, *CDKN2A* (*p16*), *CRABP1*, *IGF2*, *MLH1*, *NEUROG1*, *RUNX3*, and *SOCS1*), as previously described (Bae et al., 2017). The MethyLight assay was conducted in triplicate, and the median value was regarded as the representative value of the methylation level of each marker. The CIMP status of each tumor was defined based on the number of methylated markers as follows: CIMP-high (≥5 methylated markers), CIMP-low (1-4 methylated markers), or CIMP-0 (no methylated marker).

Droplet digital PCR

The oligonucleotide sequences of the primers and probe for RPPH1 (reference gene) were manufactured by Integrated DNA Technologies (Coralville, IA, USA). The primers and probes (*ARID1A*, *EGFR*, *FGFR1*, *KDM5B*, *MYBL2*, *MYC*, *SALL4*, and *SETDB1*) were commercially available (Life Technologies, Carlsbad, CA, USA). The copy number assay used *RPPH1* as a reference gene because of the high conservation of the

gene locus as one copy per haploid genome. The ddPCR mixture consisted of 30 ng of genomic DNA, 900 nM forward and reverse primers, 250 nM probes, and 10 µl of 2X ddPCR Supermix (Bio-Rad, Hercules, CA) in a final volume of 20 µl. A 20 µL PCR mixture and 70 µL droplet generation oil were separately loaded into adjacent wells in a QX100 Droplet Generator (Bio-Rad, Hercules, CA). The samples and oil were combined within the microchannels of the cartridge to generate an emulsion of droplets, which were then pipette-transferred to a 96-well PCR plate. ddPCR was carried out using the QX200 ddPCR system (Bio-Rad). Droplet generation and droplet reading for ddPCR were carried out according to the manufacturer's instructions (Bio-Rad). The thermal cycling conditions were 95°C for 10 min; 50 cycles of 94°C for 30 s, 60°C for 50 s, and 72°C for 30 s; 98 °C for 10 min; and a 12°C hold. Following amplification, the droplets were read using a two-color fluorescence reader (QX200 droplet reader, Bio-Rad), which determines how many droplets were positive for *ARID1A*, *EGFR*, *FGFR1*, *KDM5B*, *MYBL2*, *MYC*, *SALL4*, and *SETDB1* (in FAM) as well as for the control reaction *RPPH1* (in VIC). Each PCR plate included no-template-control (NTC) wells, which did not produce amplification signals. Data analysis was performed using QuantaSoft software version 1.7.4.0917 (Bio-Rad). Raw CN values were two times the ratio of the target sequence to a reference sequence (*RPPH1*), and CN values <1.5 and >2.5 were considered copy number variations (CNV) (Crespo et al., 2011; Wolter et al., 2022). The number of genes showing CNV among the eight target genes was counted for each CRC.

Immunohistochemistry

After tumor glass slides were reviewed under a microscope, a tissue block that was the most representative of the tumor was selected and recut. Immunohistochemistry (IHC) was performed on whole-tissue slides with an antibody against CD8 (clone SP57, Ventana Medical Systems, Tucson, AZ, USA). For the quantification of tumor-infiltrating lymphocytes (TILs), IHC slides were scanned with an Aperio AT2 slide scanner (Leica Biosystems, Vista, CA, USA). For the IHC of CDX2, KRT7, and KRT20, tumor microarray (TMA) blocks were constructed with tissue cores of 2 mm in diameter obtained from two different tumor areas. TMA blocks (n=427) were recut and immunostained with antibodies against CDX2 (clone EPR2764Y ready-to-use, CellMarque, Rocklin, CA, USA), KRT7 (CK7, clone OV-TL 12/30, Dako), and KRT20 (CK20, clone Ks20.8, Dako) using a Ventana BenchMark XT system. Based on quantification of cytoplasmic KRT7 and KRT20 and nuclear CDX2, IHC results were interpreted as follows: increased KRT7 expression and decreased KRT20 expression were determined with cutoff values set at 10% and 50%, respectively, according to a previous study (Bae et al., 2015). For the interpretation of CDX2 IHC results, the H-score, the assessment of the extent of nuclear immunoreactivity, was used and obtained with the following formula: 3 x percentage of strongly stained nuclei + 2 x percentage of moderately stained nuclei + 1 x percentage of weakly stained nuclei. The cutoff value was set at an H-score of 20, where <20 was defined as a loss of expression (Lee et al., 2022).

Quantification of tumor-infiltrating lymphocytes and tumor stromal percentage

The quantification of CD8 TILs and tumor stromal percentage (TSP) was performed as described previously (Yoo et al., 2020). In brief, the virtual slide files of CD8 IHC were used as input into an analytic pipeline (detailed protocol; https://doi.org/10.17504/protocols.io.yqvfvw6) (Yoo et al., 2020). Once the tumor area was annotated in a given image, the algorithm segmented the tumor area into 1 X 1 mm tiles and calculated the TSP and median density (number of cells/mm^2) of intraepithelial TILs (iTILs) and stromal TILs (sTILs).

Image analysis and measurement of optical density

Hematoxylin and eosin-stained whole-section slides were scanned using an Aperio AT2 slide scanner (Leica Biosystems, Wetzlar, Germany) at 20x magnification with a resolution of 0.5 µm per pixel. QuPath (Bankhead et al., 2017), an open-source solution software, was used to analyze the nuclear hematoxylin mean OD for more than 1,000 tumor cell nuclei, which were segmented by using the "Cell Detection" tool.

Statistical analysis

Statistical analysis was performed using SPSS software for Windows, version 26.0 (IBM, Armonk, NY, USA). Two-sided p values of less than 0.05 were considered statistically significant. Patients' demographic and clinical data were compared using the Student's t-test and Fisher's exact test. Continuous data with a normal distribution are expressed as the mean ± standard error, and categorical data are presented as numbers (percentages). Recurrence-free survival (RFS) was measured from the date of CRC surgery to the first documented recurrence or death from any cause, whichever came first. Survival curves were assessed using the Kaplan-Meier method and the log-rank test. Multivariate analysis was performed using the Cox proportional hazards model, and baseline characteristics were adjusted by using a backward stepwise model including covariates that were found to be significant in univariate survival analysis.

Results

A total of 437 CRCs were analyzed for their CNV statuses in eight gene markers (*ARID1A*, *EGFR*, *FGFR1*, *KDM5B*, *MYBL2*, *MYC*, *SALL4*, and *SETDB1*) using ddPCR. CIMP, MSI, *BRAF* mutation, and *KRAS*

mutation were determined in 437, 437, 432, and 425 patients, respectively. TIL density and TSP were quantified in 390 patients. The ratio of females to males was 166:271, and the mean age at surgery was 59.6 years, with a median age of 60 years (ranging from 29 to 78 years). The cancer stage was II in 71 patients and III in 366 patients. Regarding the tumor subsite within the large bowel, 135 cases involved the proximal bowel (right colon), while 273 and 29 involved the distal bowel (left colon) and the rectum, respectively. *KRAS* and *BRAF* mutations were found in 126 (29.6%) and 17 (3.9%) patients, respectively. CIMP-high and MSI-high tumors were detected in 28 (6.4%) and 32 (7.3%) patients, respectively.

Clinicopathological features of GS-like CRCs

Of the 437 CRCs, 20 (4.6%) were classified as GS-like, which were defined as MSI-low/MSS CRCs with CNVs in ≤1/8 markers, whereas 385 (88.1%) and 32 (7.3%) were classified as CIN-like CRCs and MSI-high CRCs, respectively. CIN-like CRCs were defined as tumors with MSI-low/MSS and CNV in ≥2/8 markers. Compared with CIN-like CRCs, GS-like CRCs exhibited a preponderance toward the right colon (65.0% vs. 26.5%, p=0.001) (Table 1). Age at diagnosis, sex ratio, tumor differentiation, mucinous histology, frequencies of lymphatic emboli, venous and perineural invasion, tumor depth, nodal metastasis, iTIL and sTIL densities, and TSP were similar between GS-like and CIN-like CRCs. Representative photomicrographs of each subtype are displayed in Figure 1 (A-C). In GS-like CRCs, tumor nuclei tended to be pale and hypochromatic, whereas in CIN-like CRCs, they tended to be hyperchromatic. To identify differences in the optical density (OD) of tumor nuclei between GS-like and CIN-like or MSI subtypes, the OD was assessed for more than 1,000 tumor nuclei in each case. The nuclear OD was significantly lower in GS-like than in CIN-like or MSI CRCs (Fig. 1D). Survival analysis showed no difference between the three molecular subtypes (Fig. 2).

Molecular features of GS-like CRC

Compared with CIN-like CRCs, GS-like CRCs did not show any differences in the number of mutated genes when 40 genes were analyzed by targeted exome sequencing (3.9 vs. 3.6, P=0.611). However, *KRAS* and *PIK3CA* mutations were more frequent in GS-like than in CIN-like CRCs (68.4% vs. 28.0%, P<0.001 and 43.8% vs. 14.3%, P=0.006, respectively) (Table 2). The frequency of *TP53* mutations tended to be lower in GS-

Table 1. Relationship of molecular subtype status with clinicopathological findings of stage II or III CRCs.

		n (%)	CIN-like	GS-like	MSI-high	*p* value[a]/*p* value[b]
Age	<61 years	220 (50.3)	195 (50.6)	7 (35.0)	18 (56.3)	0.251/0.163
	≥61 years	217 (49.7)	190 (49.4)	13 (65.0)	14 (43.8)	
Sex	Male	271 (62.0)	234 (60.8)	12 (60)	25 (78.1)	1.000/0.213
	Female	166 (38.0)	151 (39.2)	8 (40)	7 (21.9)	
Subsite	Proximal	135 (30.9)	102 (26.5)	13 (65)	20 (62.5)	0.001/1.000
	Distal	302 (69.1)	283 (73.5)	7 (35)	12 (37.5)	
Differentiation	Low	417 (95.4)	372 (96.6)	20	25 (78.1)	1.000/ 0.035
	High	20 (4.6)	13 (3.4)	0	7 (21.9)	
Mucin production	<50%	410 (93.8)	366 (95.1)	17 (85.0)	27 (84.4)	0.087/1.000
	≥50%	27 (6.2)	19 (4.9)	3 (15.0)	5 (15.6)	
T category	T1-3	370 (84.7)	325 (84.4)	18 (90)	27 (84.4)	0.694/0.694
	T4	67 (15.3)	60 (15.6)	2 (10)	5 (15.6)	
N category	N0	71 (16.2)	56 (14.5)	6 (30)	9 (28.1)	1.000/1.000
	N1-2	366 (83.8)	329 (85.5)	14 (70)	23 (71.9)	
Lymphatic emboli	Absent	248 (56.8)	217 (56.4)	13 (65)	18 (56.3)	0.496/0.575
	Present	189 (43.2)	168 (43.6)	7 (35)	14 (43.8)	
Venous invasion	Absent	381 (87.2)	334 (86.8)	19 (95)	28 (87.5)	0.492/0.637
	Present	56 (12.8)	51 (13.2)	1 (5)	4 (12.5)	
Perineural invasion	Absent	320 (73.4)	276 (71.9)	16 (80)	28 (87.5)	0.609/0.695
	Present	116 (26.6)	108 (28.1)	4 (20)	4 (12.5)	
iTIL	Low	195 (50)	180 (52.3)	7 (38.9)	8 (28.6)	0.336/0.530
	High	195 (50)	164 (47.7)	11 (61.1)	20 (71.4)	
sTIL	Low	195 (50)	177 (51.5)	9 (50)	9 (32.1)	1.000/0.354
	High	195 (50)	167 (48.5)	9 (50)	19 (67.9)	
TSP	Low	185 (51.1)	174 (50.6)	11 (61.1)	10 (35.7)	0.471/0.132
	High	177 (48.9)	170 (49.4)	7 (38.9)	18 (64.3)	

Percentage in parentheses; [a]GS-like vs. CIN-like; [b]GS-like vs. MSI-high.

like than in CIN-like CRCs (43.8% vs. 65.8%) but the difference did not reach statistical significance (p=0.105). The frequency of CIMP-high or CIMP-low tumors tended to be higher in GS-like than in CIN-like CRCs (10.0% vs. 4.4% and 50.0% vs. 32.7%, respectively), however, the difference did not reach statistical significance (P=0.102). GS-like CRCs showed a higher frequency of KRT7 expression than CIN-like

Table 2. Comparison of molecular features between the GS-like and CIN-like or MSI-high subtypes of CRCs

		n (%)	CIN-like	GS-like	MSI-high	p value[a]/p value[b]
BRAF	Wild type	415 (96.1)	368 (96.6)	19 (95.0)	28 (90.3)	0.517/1.000
	Mutant	17 (3.9)	13 (3.4)	1 (5.0)	3 (9.7)	
KRAS	Wild type	299 (70.4)	270 (72.0)	6 (31.6)	23 (74.2)	<0.001/0.007
	Mutant	126 (29.6)	105 (28.0)	13 (68.4)	8 (25.8)	
TP53	Wild type	135 (38.8)	105 (34.2)	9 (56.3)	21 (84.0)	0.074/0.074
	Mutant	213 (61.2)	202 (65.8)	7 (43.8)	4 (16.0)	
PIK3CA	Wild type	288 (82.8)	263 (85.7)	9 (56.3)	16 (64.0)	0.006/0.746
	Mutant	60 (17.2)	44 (14.3)	7 (43.7)	9 (36.0)	
CIMP	High	28 (6.4)	17 (4.4)	2 (10.0)	9 (28.1)	0.102/0.297
	Low	149 (34.1)	126 (32.7)	10 (50.0)	13 (40.6)	
	Zero	260 (59.5)	242 (62.9)	8 (40.0)	10 (31.3)	
KRT7	Negative	400 (93.9)	356 (95.2)	16 (80)	28 (87.5)	0.004/0.695
	Positive	26 (6.1)	18 (4.8)	4 (20)	4 (12.5)	
KRT20	Decreased	51 (12.0)	33 (8.8)	2 (10)	16 (50)	0.695/0.006
	Retained	375 (88.0)	341 (91.2)	18 (90)	16 (50)	
CDX2	Decreased	46 (10.8)	31 (8.3)	2 (10)	13 (40.6)	0.679/0.027
	Retained	381 (89.2)	344 (91.7)	18 (90)	19 (59.4)	

Percentage in parentheses; [a]GS-like vs. CIN-like; [b]GS-like vs. MSI-high.

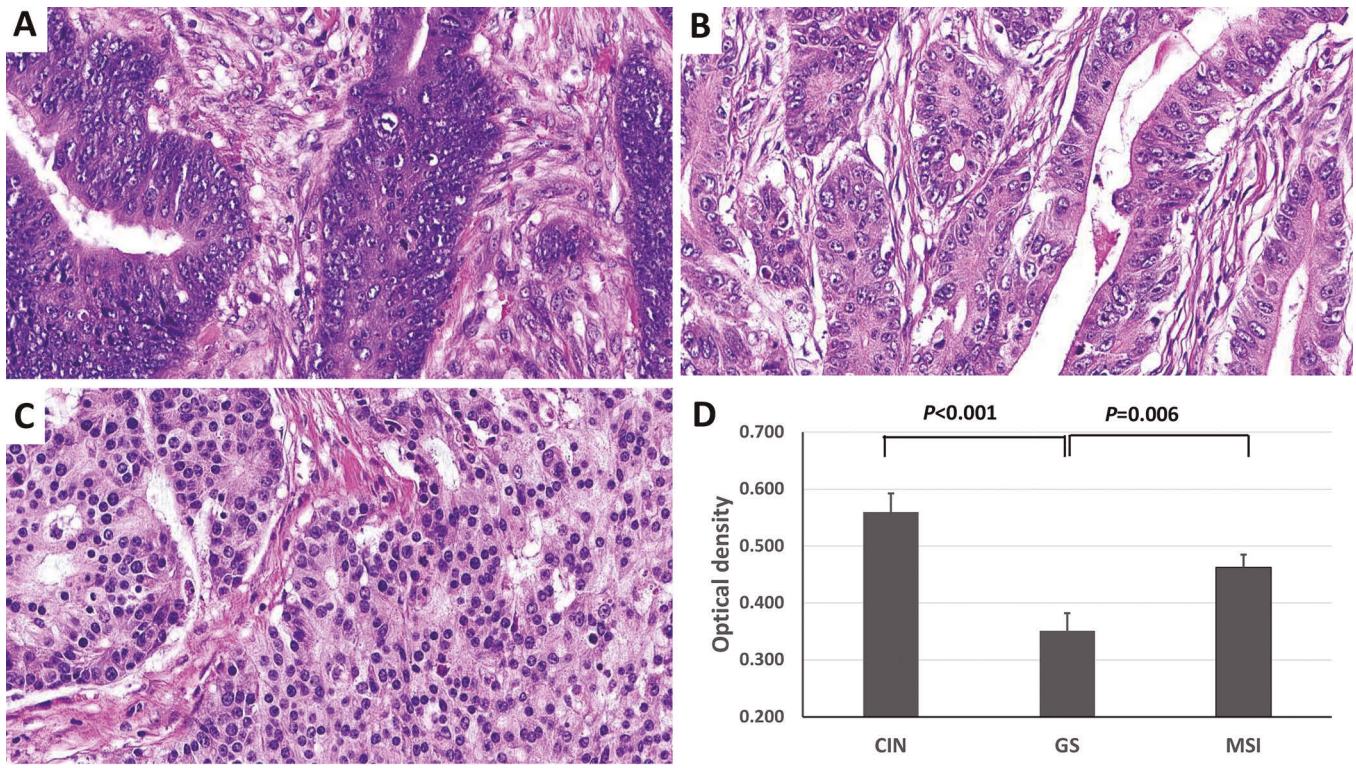

Fig. 1. Representative photomicrographs of CIN-like **(A)**, GS-like **(B)**, and microsatellite instability (MSI) **(C)** CRCs. Comparison of hematoxylin nuclear optical density of tumor nuclei among three molecular subtypes, namely, CIN-like, GS-like, and MSI **(D)**. The error bar indicates the standard error. x 400.

CRCs (20.0% vs. 4.8%, *P*=0.020), but no difference in the frequency of KRT20 or CDX2 loss between GS-like and CIN-like CRCs was observed.

Discussion

In the present study, we analyzed a cohort of stage III or high-risk stage II CRCs (n=437) for their CNV status in eight genes using ddPCR and then classified them into CIN-like, GS-like, and MSI-high CRCs based on both MSI and the number of genes exhibiting CNV. GS-like, CIN-like, and MSI-high CRCs comprised 4.6%, 88.1%, and 7.3% of the cohort, respectively. Compared with CIN-like CRCs, GS-like CRCs featured a proximal colon location, lower nuclear OD, and higher frequencies of *KRAS* and *PIK3CA* mutations and KRT7 expression. However, no difference was noted in clinicopathological features between CIN-like and GS-like CRCs, including mucinous histology, tumor differentiation, frequency of lymphovascular emboli or perineural invasion, age at diagnosis, sex ratio, T and N categories, density of TILs, and survival of patients.

In 2014, TCGA classified gastric carcinomas (GCs) into EBV-positive, MSI-high, CIN, and GS subtypes based on a comprehensive molecular characterization of DNA, RNA, and protein from resected GC tissues (Cancer Genome Atlas Research, 2014). GS GCs are histologically distinct and differentiated from CIN or MSI GCs by the enrichment of the diffuse histological subtype, whereas CIN or MSI GCs feature the intestinal histological subtype. For GCs, molecular subtypes showed an association with prognosis, and GS GCs had the worst prognosis (Sohn et al., 2017). In contrast with GS GCs, GS CRCs did not show any characteristic histological features distinct from CIN or MSI CRCs. Based on the high frequency of *APC* mutations in GS CRCs, the Laird team suggested that GS CRCs might develop along the classic adenoma-carcinoma pathway, which might explain why there is no difference in histological features between GS and CIN tumors (Liu et al., 2018). However, tumor nuclei of GS-like CRCs showed a lower OD than those of CIN-like or MSI CRCs. Because OD is the measure of absorbance of light through a sample, nuclear hematoxylin OD is

Table 3. Univariate and multivariate analyses of combinatory statuses of *KRAS* and *PIK3CA* mutations regarding RFS of CRC patients.

Parameter	Univariate analysis		Multivariate analysis[a]	
	HR (95% CI)	*p* value	HR (95% CI)	*p* value
KRAS/PIK3CA wild type	1		1	
PIK3CA mutation alone	1.453 (0.514-4.110)	0.481	1.983 (0.676-5.818)	0.213
KRAS mutation in exon 2	1.594 (0.933-2.725)	0.088	1.907 (1.065-3.416)	0.030
Mutations in both *KRAS* exon 2 and *PIK3CA*	0.650 (0.230-1.838)	0.417	0.688 (0.207-2.286)	0.541
KRAS mutation in exon 3 or 4	0.652 (0.089-4.774)	0.674	0.724 (0.098-5.364)	0.752
Mutations in both *KRAS* exon 3 or 4 and *PIK3CA*	1.020 (0.139-7.468)	0.984	0.678 (0.086-5.331)	0.712

[a]Adjusted for tumor differentiation, lymphatic embolus, venous invasion, perineural invasion, T category, N category, and CD8 iTIL.

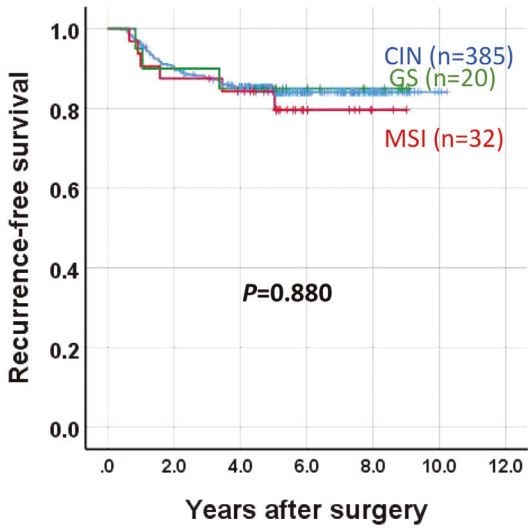

Fig. 2. Recurrence-free survival according to the molecular subtypes of CRC. Kaplan-Meier survival curves for CIN, GS, and MSI CRCs.

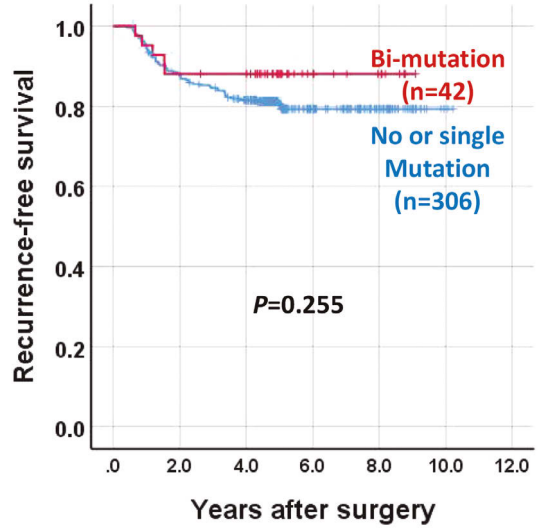

Fig. 3. Kaplan-Meier survival curves for CRCs with mutations in both *KRAS* and *PIK3CA* and CRCs with a single or no mutation in *KRAS* and *PIK3CA*.

proportional to hyperchromatism. Thus, as reflected in the higher and lower OD in the tumor nuclei, CIN-like CRCs tended to be hyperchromatic, and those of the GS-like CRCs tended to be pale and vesicular.

According to the study by the Laird team (Liu et al., 2018), GS CRCs featured a high frequency of *KRAS* and *PIK3CA* mutations. In the present study, concomitant mutation of *KRAS* and *PIK3CA* was one of the molecular features of GS-like CRCs and was twice as frequent in GS-like than CIN-like or MSI CRCs (37.5% vs. 10.1% or 16.0%, respectively, $p<0.001$). Concomitant mutations of *KRAS* and *PIK3CA* indicate activation of both the mitogen-activated protein kinase (MAPK) and phosphatidyl-inositol-3 kinase (PI3K) pathways. Luo et al. (2020) found concomitant mutations of *KRAS* and *PIK3CA* in 8.4% of CRCs (n=655) and reported that tumors with both *KRAS* and *PIK3CA* mutations showed a predilection toward a proximal bowel location, poor differentiation, and a shortened overall survival time. However, in the present study, CRCs with both *KRAS* and *PIK3CA* mutations showed an association with a proximal location but did not show an association with shortened survival (Fig. 3). When we further divided *KRAS* mutations into exon 2 and or exons 3 and 4 mutations, mutations in both *KRAS* exon 2 and *PIK3CA* showed an association with poor survival in univariate analysis; however, neither mutations of both *KRAS* exon 2 and *PIK3CA* nor mutations in both *KRAS* exon 3/4 and *PIK3CA* showed an association with poor survival in multivariate analysis (Table 3).

CIN is a common molecular feature of CRCs, however, there is no clear consensus on how to diagnose CIN in CRCs. Different methods, such as karyotyping (Sajesh et al., 2013), fluorescence *in situ* hybridization (Penner-Goeke et al., 2017), comparative genomic hybridization (Bakker et al., 2016), NGS (Greene et al., 2016), and IHC (Li et al., 2020), have been used to diagnose CIN in CRCs, and each method has its strengths and limitations (Lepage et al., 2019). NGS is the most accurate tool for the diagnosis of CIN but requires expensive equipment and a specialized workforce. In the present study, we utilized ddPCR to assess CNV status in eight markers and regarded MSS or MSI-low CRCs with ≤1 altered marker as GS-like CRCs. Whether the eight genes selected are truly the most appropriate markers for the diagnosis of GS CRCs is a limitation of this study that should be acknowledged. Nevertheless, GS-like CRCs defined by ddPCR shared clinicopathological and molecular features in common with GS CRCs defined by the NGS-based study of Liu et al. (2018), including proximal tumor location and high frequency of *KRAS* and *PIK3CA* mutations.

In conclusion, we analyzed stage III and high-risk stage II CRCs for their CNV status in eight genes, finding that GS-like CRCs comprised a minor proportion of CRCs and featured high frequencies of KRT7 expression and mutations in both *KRAS* and *PIK3CA*. Except for the proximal location and hypochromatic nuclei of tumor cells, no differences were identified in clinicopathological features between CIN-like and GS-like CRCs.

Declaration of conflict of interest. The authors declare no competing interests.

Funding. This study was supported by grants from the National Research Foundation of Korea (NRF) funded by the Korean Government (MSIT) (No. 2021R1A2C1003542 and RS-2023-00218623).

References

Al-Sohaily S., Biankin A., Leong R., Kohonen-Corish M. and Warusavitarne J. (2012). Molecular pathways in colorectal cancer. J. Gastroenterol. Hepatol. 27, 1423-1431.

Bae J.M., Lee T.H., Cho N.Y., Kim T.Y. and Kang G.H. (2015). Loss of CDX2 expression is associated with poor prognosis in colorectal cancer patients. World J. Gastroenterol. 21, 1457-1467.

Bae J.M., Kim J.H. and Kang G.H. (2016). Molecular subtypes of colorectal cancer and their clinicopathologic features, with an emphasis on the serrated neoplasia pathway. Arch. Pathol. Lab. Med. 140, 406-412.

Bae J.M., Kim J.H., Kwak Y., Lee D.W., Cha Y., Wen X., Lee T.H., Cho N.Y., Jeong S.Y., Park K.J., Han S.W., Lee H.S., Kim T.Y. and Kang G.H. (2017). Distinct clinical outcomes of two CIMP-positive colorectal cancer subtypes based on a revised CIMP classification system. Br. J. Cancer 116, 1012-1020.

Bakker B., Taudt A., Belderbos M.E., Porubsky D., Spierings D.C., de Jong T.V., Halsema N., Kazemier H.G., Hoekstra-Wakker K., Bradley A., de Bont E.S., van den Berg A., Guryev V., Lansdorp P.M., Colome-Tatche M. and Foijer F. (2016). Single-cell sequencing reveals karyotype heterogeneity in murine and human malignancies. Genome Biol. 17, 115.

Bankhead P., Loughrey M.B., Fernandez J.A., Dombrowski Y., McArt D.G., Dunne P.D., McQuaid S., Gray R.T., Murray L.J., Coleman H.G., James J.A., Salto-Tellez M. and Hamilton P.W. (2017). Qupath: Open source software for digital pathology image analysis. Sci. Rep. 7, 16878.

Cancer Genome Atlas Research N. (2014). Comprehensive molecular characterization of gastric adenocarcinoma. Nature 513, 202-209.

Colussi D., Brandi G., Bazzoli F. and Ricciardiello L. (2013). Molecular pathways involved in colorectal cancer: Implications for disease behavior and prevention. Int. J. Mol. Sci. 14, 16365-16385.

Crespo I., Vital A.L., Nieto A.B., Rebelo O., Tao H., Lopes M.C., Oliveira C.R., French P.J., Orfao A. and Tabernero M.D. (2011). Detailed characterization of alterations of chromosomes 7, 9, and 10 in glioblastomas as assessed by single-nucleotide polymorphism arrays. J. Mol. Diagn. 13, 634-647.

Greene S.B., Dago A.E., Leitz L.J., Wang Y., Lee J., Werner S.L., Gendreau S., Patel P., Jia S., Zhang L., Tucker E.K., Malchiodi M., Graf R.P., Dittamore R., Marrinucci D. and Landers M. (2016). Chromosomal instability estimation based on next generation sequencing and single cell genome wide copy number variation analysis. PLoS One 11, e0165089.

Jass J.R. (2007). Classification of colorectal cancer based on correlation of clinical, morphological and molecular features. Histopathology 50, 113-130.

Jass J.R., Walsh M.D., Barker M., Simms L.A., Young J. and Leggett B.A. (2002). Distinction between familial and sporadic forms of colorectal cancer showing DNA microsatellite instability. Eur. J. Cancer 38, 858-866.

Jin H.Y., Yoo S.Y., Lee J.A., Wen X., Kim Y., Park H.E., Kwak Y., Cho N.Y., Bae J.M., Kim J.H., Lee H.S. and Kang G.H. (2022). Combinatory statuses of tumor stromal percentage and tumor infiltrating lymphocytes as prognostic factors in stage iii colorectal cancers. J. Gastroenterol. Hepatol. 37, 551-557.

Jung K.W., Won Y.J., Kang M.J., Kong H.J., Im J.S. and Seo H.G. (2022). Prediction of cancer incidence and mortality in korea, 2022. Cancer Res. Treat. 54, 345-351.

Lee D.W., Han S.W., Cha Y., Bae J.M., Kim H.P., Lyu J., Han H., Kim H., Jang H., Bang D., Huh I., Park T., Won J.K., Jeong S.Y., Park K.J., Kang G.H. and Kim T.Y. (2017). Association between mutations of critical pathway genes and survival outcomes according to the tumor location in colorectal cancer. Cancer 123, 3513-3523.

Lee J.A., Seo M.K., Yoo S.Y., Cho N.Y., Kwak Y., Lee K., Kim J.H. and Kang G.H. (2022). Comprehensive clinicopathologic, molecular, and immunologic characterization of colorectal carcinomas with loss of three intestinal markers, CDX2, SATB2, and KRT20. Virchows Arch. 480, 543-555.

Leggett B. and Whitehall V. (2010). Role of the serrated pathway in colorectal cancer pathogenesis. Gastroenterology 138, 2088-2100.

Lepage C.C., Morden C.R., Palmer M.C.L., Nachtigal M.W. and McManus K.J. (2019). Detecting chromosome instability in cancer: Approaches to resolve cell-to-cell heterogeneity. Cancers 11, 226.

Li Y., Li J., Guo E., Huang J., Fang G., Chen S., Yang B., Fu Y., Li F., Wang Z., Xiao R., Liu C., Huang Y., Wu X., Lu F., You L., Feng L., Xi L., Wu P., Ma D., Sun C., Wang B. and Chen G. (2020). Integrating pathology, chromosomal instability and mutations for risk stratification in early-stage endometrioid endometrial carcinoma. Cell Biosci. 10, 122.

Liu Y., Sethi N.S., Hinoue T., Schneider B.G., Cherniack A.D., Sanchez-Vega F., Seoane J.A., Farshidfar F., Bowlby R., Islam M., Kim J., Chatila W., Akbani R., Kanchi R.S., Rabkin C.S., Willis J.E., Wang K.K., McCall S.J., Mishra L., Ojesina A.I., Bullman S., Pedamallu C.S., Lazar A.J., Sakai R., Cancer Genome Atlas Research N., Thorsson V., Bass A.J. and Laird P.W. (2018). Comparative molecular analysis of gastrointestinal adenocarcinomas. Cancer Cell 33, 721-735 e728.

Luo Q., Chen D., Fan X., Fu X., Ma T. and Chen D. (2020). KRAS and PIK3CA bi-mutations predict a poor prognosis in colorectal cancer patients: A single-site report. Transl. Oncol. 13, 100874.

McGranahan N., Burrell R.A., Endesfelder D., Novelli M.R. and Swanton C. (2012). Cancer chromosomal instability: Therapeutic and diagnostic challenges. EMBO Rep. 13, 528-538.

Nguyen L.H., Goel A. and Chung D.C. (2020). Pathways of colorectal carcinogenesis. Gastroenterology 158, 291-302.

Penner-Goeke S., Lichtensztejn Z., Neufeld M., Ali J.L., Altman A.D., Nachtigal M.W. and McManus K.J. (2017). The temporal dynamics of chromosome instability in ovarian cancer cell lines and primary patient samples. PLoS Genet. 13, e1006707.

Pino M.S. and Chung D.C. (2010). The chromosomal instability pathway in colon cancer. Gastroenterology 138, 2059-2072.

Sajesh B.V., Lichtensztejn Z. and McManus K.J. (2013). Sister chromatid cohesion defects are associated with chromosome instability in hodgkin lymphoma cells. BMC Cancer 13, 391.

Satorres C., Garcia-Campos M. and Bustamante-Balen M. (2021). Molecular features of the serrated pathway to colorectal cancer: Current knowledge and future directions. Gut Liver 15, 31-43.

Shia J., Schultz N., Kuk D., Vakiani E., Middha S., Segal N.H., Hechtman J.F., Berger M.F., Stadler Z.K., Weiser M.R., Wolchok J.D., Boland C.R., Gonen M. and Klimstra D.S. (2017). Morphological characterization of colorectal cancers in The Cancer Genome Atlas reveals distinct morphology-molecular associations: Clinical and biological implications. Mod. Pathol. 30, 599-609.

Sohn B.H., Hwang J.E., Jang H.J., Lee H.S., Oh S.C., Shim J.J., Lee K.W., Kim E.H., Yim S.Y., Lee S.H., Cheong J.H., Jeong W., Cho J.Y., Kim J., Chae J., Lee J., Kang W.K., Kim S., Noh S.H., Ajani J.A. and Lee J.S. (2017). Clinical significance of four molecular subtypes of gastric cancer identified by the cancer genome atlas project. Clin. Cancer Res. 23, 4441-4449.

Spittle C., Ward M.R., Nathanson K.L., Gimotty P.A., Rappaport E., Brose M.S., Medina A., Letrero R., Herlyn M. and Edwards R.H. (2007). Application of a BRAF pyrosequencing assay for mutation detection and copy number analysis in malignant melanoma. J. Mol. Diagn. 9, 464-471.

Sung H., Ferlay J., Siegel R.L., Laversanne M., Soerjomataram I., Jemal A. and Bray F. (2021). Global Cancer Statistics 2020: GLOBOCAN estimates of incidence and mortality worldwide for 36 cancers in 185 countries. CA Cancer J. Clin. 71, 209-249.

Trautmann K., Terdiman J.P., French A.J., Roydasgupta R., Sein N., Kakar S., Fridlyand J., Snijders A.M., Albertson D.G., Thibodeau S.N. and Waldman F.M. (2006). Chromosomal instability in microsatellite-unstable and stable colon cancer. Clin. Cancer Res. 12, 6379-6385.

Wolter M., Felsberg J., Malzkorn B., Kaulich K. and Reifenberger G. (2022). Droplet digital PCR-based analyses for robust, rapid, and sensitive molecular diagnostics of gliomas. Acta Neuropathol. Commun. 10, 42.

Yoo S.Y., Park H.E., Kim J.H., Wen X., Jeong S., Cho N.Y., Gwon H.G., Kim K., Lee H.S., Jeong S.Y., Park K.J., Han S.W., Kim T.Y., Bae J.M. and Kang G.H. (2020). Whole-slide image analysis reveals quantitative landscape of tumor-immune microenvironment in colorectal cancers. Clin. Cancer Res. 26, 870-881.

Accepted June 25, 2024